European Polymer Journal 225 (2025) 113728

Contents lists available at ScienceDirect

European Polymer Journal

journal homepage: www.elsevier.com/locate/europolj

Eco-design of biobased poly(butylene succinate-b-pentamethylene 2,5-furanoate) copolymers with optimized mechanical, thermal and barrier properties for flexible food-packaging

Mattia Manfroni [a,1], Alessandro Coatti [a,1], Michelina Soccio [a,b,c,*], Valentina Siracusa [d], Elisa Boanini [e], Elisabetta Salatelli [f], Nadia Lotti [a,b,g]

[a] Department of Civil, Chemical, Environmental and Materials Engineering, University of Bologna, Via, Terracini 28, Bologna 40131, Italy
[b] Interdepartmental Center for Industrial Research on Advanced Applications in Mechanical Engineering and Materials Technology, CIRI-MAM, Viale del Risorgimento 2, 40136, Bologna, Italy
[c] Interdepartmental Center for Industrial Research on Buildings and Construction CIRI-EC, Via del Lazzaretto 15/5, 40131, Bologna, Italy
[d] Department of Chemical Science, University of Catania, Viale A, Doria 6, Catania 95125, Italy
[e] Department of Chemistry "Giacomo Ciamician", University of Bologna, Via, Selmi 2, Bologna 40126, Italy
[f] Department of Industrial Chemistry "Toso Montanari", University of Bologna, Viale, Risorgimento 4, 40136 Bologna, Italy
[g] Interdepartmental Center for Industrial Agro-Food Research, CIRI-AGRO, Via, Quinto, Bucci 336, 47521, Cesena, Italy

ARTICLE INFO

Keywords:
Poly(butylene succinate)
2,5-furan dicarboxylic acid
Block copolymers
Flexible packaging
Sustainability

ABSTRACT

Poly(butylene succinate) and poly(pentamethylene 2,5-furanoate) homopolymers have been combined, both physically as well as chemically, to optimize the final material's functional properties for flexible food packaging applications. The two parent homopolymers were synthesized through two-step bulk polycondensation, then they were physically mixed in an equiponderal blend by solvent casting. The blend was subjected to reactive blending at high temperature and in presence of the catalyst, for different times, to prepare several copolymers with tuned molecular architecture, i.e. different block lengths. After molecular characterization, the polymers were processed in form of films and subjected to thermal (TGA and DSC), structural (SEM and XRD), mechanical and gas barrier characterization. All the materials show very high thermal stability (T_{onset} > 360 °C; T_{max} > 390 °C) and modulated melting temperatures (43 °C < T_m < 113 °C). Even if not miscible, the two homopolymers reveal good compatibility, reflected in enhanced flexibility (elastic modulus reduced up to one order of magnitude) and elongation (up to five times higher) already in the physical blend, together with surprising elastic capability in the copolymers (shape recovery > 70 %). The presence of furan moieties in the final materials leads to reduced permeability of CO_2 and, particularly, of O_2 (up to Barrier Improvement Factor (BIF) ≈ 8). The results obtained highlight the possibility of modulating the material response by playing with composition and repeating unit distribution along the macromolecules.

1. Introduction

The surge in plastics production in recent years has outpaced the growth of any other material. Over 400 million tons of plastics are produced annually worldwide [1]. Plastics production is estimated to exceed 1 billion tons during the 2050–2060 decade [2]. On the other hand, the prospect of a world devoid of plastics, or synthetic organic polymers, appears unfathomable in the contemporary context. The valuable role of plastics is recognized by their versatility across numerous applications, due to their inherent properties like low cost, lightness, processability, non-reactivity, durability and resistance to degradation. Unfortunately, some of these qualities turn plastics recalcitrant or impermeable to natural assimilation causing environmental issues, particularly in terms of impact on ocean, wildlife and human health [3]. In addition, the absence of a well-defined approach to waste management, comprehending both disposal and incineration, is the main reason for the uncontrolled accumulation of plastics throughout all principal terrestrial and aquatic ecosystems, on a planetary scale [4,5].

* Corresponding author.
E-mail address: m.soccio@unibo.it (M. Soccio).
[1] These authors contributed equally.

https://doi.org/10.1016/j.eurpolymj.2025.113728
Received 29 October 2024; Received in revised form 20 December 2024; Accepted 4 January 2025
Available online 6 January 2025

Furthermore, the majority of plastic waste could be associated with materials coming from non-renewable resources which contributes dramatically to source depletion and pollution. Plastic materials are extensively utilized in packaging, with food packaging accounting for more than half of the plastics used in this area [6]. At the same time, packaging is the sector where plastic materials have the shortest life-span. Recently, flexible-type packaging experienced rapid growth, in particular, within this sector, where an important component of modern food packaging is represented by plastic films, defined as materials with thicknesses up to 250 μm [7]. In this context, the need to reduce the environmental impact coming from the production and the accumulation of petroleum-based plastics by using alternative polymers while maintaining identical or superior performance is critical. In 2018, the European Commission (EC) introduced Directive 94/62, which outlined long-term circular economy targets. The directive stipulates that 65 % of total packaging waste should be recycled by 2025, to reach 70 % by 2030 [8]. Thus, EC considers the enhancement of recycling strategies as a key point in transitioning towards a circular economy. Recycling, instead of the other possibilities, offers the advantage of preserving the properties of materials while minimizing the environmental impact of plastic waste. Concerning food-packaging applications, in which often single-use is the main consumption pattern, the recycling route is a major challenge due to problems related to the removal of possible organic contaminants and due to the evolution of flexible packaging into thin, multi-layer structures (i.e. multilayered films with several sheets containing also ethylene vinyl alcohol (EVOH) to guarantee high barrier properties) [9]. One of the strategies to overcome these limitations is to redesign packages using monolayered structures that facilitate recycling. A progressive rise of interest in bioplastics as packaging solutions has been witnessed in recent past years. Bioplastics are plastic materials that are either entirely or partially derived from natural sources (bio-based) and/or biodegradable due to the action of microorganisms. The use of bioplastics not only aims to reduce no-renewable source consumption but also offers potential benefits in terms of the nature of the building blocks, being sustainable and climate-friendly, and in terms of biodegradability and reduction of carbon footprint [10]. Unfortunately, according to the European Bioplastics Association (EUBP), the global production capacity of biobased plastics reached 2.18 million tons in 2023 which still represents less than 1 % of global plastics production [11]. Currently, just a few bioplastics are used in packaging. Among them, there are polyesters such as poly(lactic acid) (PLA) which can be both biobased and biodegradable, and poly(butylene adipate-*co*-terephthalate) (PBAT), a compostable material for films and bags available on the market under the name Ecoflex [12]. Poly(butylene succinate) (PBS) is considered one of the most valuable biobased aliphatic polyesters, characterized by good thermo-mechanical properties, low production costs and a wide workability window, one of the largest among the aliphatic polyesters. It derives from the combination of succinic acid (SA) and 1,4-butanediol (1,4-BD). Interest in PBS has significantly increased for applications that require a balance between mechanical strength and flexibility [13]. PBS can act as a reinforcing agent or a plasticizer in blends with other polymers. Its compatibility can be improved by incorporating a PBS copolymer that acts as a bridging agent between phases. This approach is effective when mixed with materials that lack functional groups, such as PE, PP, PS or polycaprolactone (PCL). Liu et al. investigated a blend of PBS with 20 wt% PCL and found that a satisfactory level of miscibility is achieved by incorporating the PBS-*co*-PCL copolymer as a compatibilizer [14]. To enhance compatibility, a low molecular weight initiator can be used to promote the formation of covalent bonds between phases. For example, in the blend of PBS and polyhydroxyalkanoates (PHAs), dicumyl peroxide (DCP) is utilized [15]. The latter is also used in PBS and PLA blends, where the peroxide aids in forming the PLA-*co*-PBS copolymer, thereby reducing the interfacial tension between the two phases [16]. Other polymers extensively studied in blends with PBS include natural compounds, such as several cellulose and lignin derivatives [17,18], as well as synthetic biodegradable polymers like PBAT [19]. PBS homopolyester represents a good candidate for packaging applications in general, but in the food sector, it lacks the required barrier properties. Gas permeability through food packaging is directly correlated with the quality and safety of the packaged products. Oxygen ingress can result in oxidation, while carbon dioxide leakage can compromise the effectiveness of modified atmosphere packaging [7]. Polyesters derived from 2,5-furandicarboxylic acid (FDCA), one of the 12 building blocks of the future [20], have proved to be very interesting biobased polymers due to their functional properties, in particular, outstanding gas-barrier ability. Poly(ethylene furan-2,5-dicarboxylate) (PEF) exhibits superior mechanical and gas barrier properties compared to PET, and poly(pentamethylene 2,5-furanoate) (PPeF) is even more promising [21,22]. PPeF's thermal properties show a predominantly amorphous character, while the mechanical response recalls an elastomeric behaviour [23,24]. There are also several studies on other homopolyesters, copolymers and composite materials based on 2,5-furandicarboxylic acid. A series of homopolyesters have been synthetized using medium-short chain aliphatic glycols (up to C8) observing the variability of the mechanical and thermal properties [25,26]. Bikiaris et al. explored longer-chain glycols obtaining more ductile hompolyesters [27]. Furthermore, Lopez-Sanchez et al., have integrated a polyester based on FDCA, SA, 1,3-propanediol and 1,5-pentanediol with a biobased cyclic structure like isosorbide (ISB) finding an increased rigidity [28]. In this research, we explored the combination of the favourable thermo-mechanical properties of PBS with the excellent barrier properties and elastic behavior of PPeF, both polymers being fully biobased, to create a single-layer material suitable for use in flexible food packaging. We investigated the thermal, mechanical, and barrier properties of an equiponderal PBS/PPeF blend and a range of block copolymers derived from it. Although our focus was not on biodegradability, it's worth noting that PBS is not only derived from biomass but also biodegradable. Moreover, some of us have found the possibility of composting PPeF films [29]. That means that when mechanical recycling is hampered by organic contaminants or is not feasible, biodegradability and chemical recycling could be viable alternatives.

2. Materials and methods

2.1. Materials

Dimethyl furan-2,5-dicarboxylate (DMF) was provided by Sarchem Labs (purity 99.8 %). 1,5-pentanediol (PD) (97 %), 1,4-butanediol (1,4-BD) (99 %), DBE-4 dibasic ester (98 %), titanium tetrabutoxide (TBT), titanium isopropoxide (TIP), and chloroform (purity $\geq$ 99.8 %) were purchased from Sigma-Aldrich. All the reagents were used without any further purification.

2.2. Synthesis of homopolyesters

Aliphatic poly(butylene succinate) (PBS) and aromatic poly(pentamethylene 2,5-furanoate) (PPeF) were prepared by the well-known bulk two-step polycondensation process. The reaction was conducted in a 250 mL thermostatted stirred glass reactor. To obtain PBS homopolymer the reactor was charged with the reagents DBE-4 dibasic ester and 1,4-butanediol in a 1/1.2 M ratio, respectively, together with TBT as catalyst (400 ppm). The first step was carried out in an inert N_2 atmosphere and continuous stirring (50 rpm) at 190 °C. During this first stage, transesterification took place with the release of methanol which was removed from the reaction mixture by distillation and collected in a glass trap downstream of the reactor. Transesterification was considered completed once 90 % of theoretical MeOH was collected, i.e. after 90 min. In the second polycondensation step, the reacting system was gradually heated to 220 °C and the pressure was simultaneously reduced to 0.05 mbar. The second stage was concluded after 3.5 h, once a constant torque value was measured. Finally, the polymer was easily

discharged from the reactor and stored at room temperature. PPeF polymer was prepared following the same procedure used for PBS. The process involved the use of a 250 mL thermostatted stirred glass reactor charged with the reagents dimethyl furan-2,5-dicarboxylate and 1,5-pentanediol in a 1/1.5 M ratio, respectively, along with the catalysts (TBT 200 ppm and TIP 200 ppm). The first and second step times were 90 min and 4.0 h, respectively.

2.3. Blend preparation

PBS and PPeF were wholly dissolved in chloroform under magnetic stirring at room temperature (4 h) to obtain a homogeneous mixture (50/50 wt/wt) of the parent homopolymers. The resulting solution was then cast onto a Petri dish, and the solvent was let to evaporate at room temperature. The equiponderal physical blend hereafter will be indicated as PBS/PPeF. The process described, solution mixing and casting, ensures the obtainment of a physical blend, allowing to avoid transesterification reactions between PBS and PPeF that would take place at high temperatures during melt mixing.

2.4. Copolymer synthesis

Block copolymers were synthesized starting from PBS/PPeF physical mixture through reactive blending carried out in bulk employing a glass reactor under a nitrogen atmosphere at 220 °C. Different mixing times were selected to obtain copolymers with different block lengths. The samples were designated as P(BS-*b*-PeF)$_x$ where *x* represents the corresponding mixing time.

2.5. Molecular characterization

2.5.1. Nuclear magnetic resonance (NMR)

^{1}H NMR and ^{13}C NMR spectroscopy have been used for the determination of chemical structure, composition and randomness degree. The samples were prepared by dissolving (10 and 30 mg ml^{-1} for ^{1}H- and ^{13}C NMR, respectively) in deuterated chloroform with TMS (0.03 vol%) as an internal reference. The measurements were recorded with a Varian XL-400 NMR spectrometer (Palo Alto, CA, USA) at 25 °C. ^{1}H NMR spectra were recorded adopting a relaxation delay of 0 s, an acquisition time of 1 s, and up to 100 repetitions. ^{13}C NMR spectra were obtained using a relaxation delay of 1 s, an acquisition time of 1 s, and up to 700 repetitions.

2.5.2. Gel permeation chromatography (GPC)

Molecular weights were determined by gel-permeation chromatography (GPC) at 30 °C using an HPLC Lab Flow 2000 apparatus (KNAUER, Berlin, Germany) equipped with a Rheodyne 7725i injector, a column inlet filter 7335 Rheodyne, a Phenomenex MXM 5 μm mixed bed column, and a RI K-2301 KNAUER detector. Chloroform was used as the mobile phase (1.0 mL min^{-1} flow) of injected polymer solutions (2 mg ml^{-1}). Monodisperse polystyrene standards (Sigma Aldrich Chemical Co., St. Louis, MO, USA) were used to build the calibration curve.

2.6. Structural & morphological characterization

2.6.1. X-ray diffraction (XRD)

The nature and amount of crystalline phases were determined using a wide-angle X-ray scattering (WAXS), with a PANanalytical X'Pert PRO diffractometer equipped with an X'Celerator detector and a copper target. The analysis has been conducted at room temperature in the 3-60° 2θ range (acquisition time of 100 s/step; step of 0.10°). The degree of crystallinity for each sample was determined as the ratio between the crystalline peak area and the entire area under the diffractometric curve.

2.6.2. Scanning electron microscope (SEM)

The microstructure and the morphology of each sample were investigated using a Zeiss Leo-1530 scanning electron microscope, operating at an accelerating voltage of 5 kV (secondary electrons). The cryo-fractured cross-section of the polymeric films was analyzed after gold metallization through physical vapor deposition (PVD).

2.7. Film preparation

Circular polymeric films with a diameter of approximately 11 cm and an average thickness of 150 μm were prepared by compression moulding using a laboratory press Carver C12. The as-synthesized polymers, as well as the physical blend, were put into two Teflon sheets and heated at 40 °C above the relative melting temperature (or glass transition temperature in the case of amorphous PPeF). Once molten, a pressure of 8 tons/m^2 was applied for 2 min. Finally, films were cooled down (through water cooling coils) to room temperature and stored for 10 days before further characterization to attain the equilibrium crystallinity.

2.8. Thermal analysis

2.8.1. Thermogravimetric analysis (TGA)

The thermal stability of the prepared samples was investigated through thermogravimetric analysis using a PerkinElmer TGA4000. The measurements were carried out under N_2 flow (40 ml min^{-1}) by heating 5 mg of polymer from 40 to 800 °C at 10 °C min^{-1}. The temperature of initial degradation (T_{onset}) and the temperature corresponding to the maximum degradation rate (T_{max}) were determined.

2.8.2. Differential scanning Calorimetry (DSC)

DSC analysis was employed to determine the main thermal transitions in the polymer samples when subjected to a predetermined thermal program. Measurements were conducted with a Pyris DSC6 calorimeter (PerkinElmer, Shelton, CT, USA) under nitrogen flux (20 mL min^{-1}) using the following thermal program: ≈ 5 mg of polymer film were brought to −60 °C and heated up to 150 °C at 20 °C min^{-1} (I scan), held there for 3 min, and then rapidly cooled (100 °C min^{-1}) to − 60 °C. Finally, it was reheated from − 60 °C to a temperature 40 °C above the melting point of the sample with a heating rate of 20 °C/min (II scan). The glass transition temperature (T_g) was calculated as the midpoint of the glass-to-rubber transition step. At the same time, the specific heat increment (ΔC_p) was obtained from the jump height between the two baselines associated with the glass transition step. Melting temperature (T_m) was taken at the peak maximum of the melting endotherm. The heat of fusion (ΔH_m) of the crystalline phase was calculated from the total area of the DSC endotherm. In the same way, also the cold crystallization temperature (T_{cc}) and the corresponding enthalpy (ΔH_{cc}) have been evaluated.

2.9. Stress–strain measurements

Polymer's rectangular films (5 × 20 mm^2) were characterized from a mechanical point of view through an Instron 5966 dynamometer (Norwood, MA, USA) equipped with a rubber grip and a transducer-coupled 10 kN loading cell controlled by a computer. The tests were conducted at room temperature and relative humidity of 50 % with a gauge length of 20 mm and a strain rate of 10 mm/min until breaking. Tensile elastic modulus (E), from the initial linear slope of the stress–strain curve, elongation at break (ε_b), and stress at break (σ_b) were determined. At least five specimens for each sample were tested and the results were reported as the average value ± standard deviation. Cyclic loading analysis was also performed to evaluate the elastic return: samples without yielding points were strained and released (20 cycles at 10 mm/min) to get 5–30 % elongation.

2.10. Gas barrier analysis

Gas-barrier performance was evaluated by a manometric method using a Brugger Feinmechanik GmbH (Munich, Germany) GDP-C type Permeance Testing Apparatus, following the ASTM 1434-82 standard (the relative standard procedure for the determination of gas-barrier properties of polymeric films). The tests complied with DIN 53 536 and ISO/DIS 15 105–1, and the corresponding gas permeability manual (Registergericht München HRB 77020, Brugger Feinmecha-nik GmbH). The lower chamber was initially brought into a high vacuum condition; after which the upper chamber was filled with the gas to be studied, with a filling speed of 100 cm^3/min. In the lower chamber, there was a pressure transducer, which continuously recorded the increase in gas pressure as a function of time. The gas transmission rate (GTR), expressed in cm^3 cm m^{-2} d^{-1} atm^{-1} was determined by evaluating the speed of pressure increase, taking into account the chamber volume and normalizing with respect to film thickness. The permeability values to dry O_2 and CO_2 (RH = 0 %), food grade, at a standard temperature (r.t. = 23 °C) were determined. The gas transmission measurements were conducted in triplicate to ensure accuracy and precision. The calculated mean values have been presented as the average ± standard deviation.

3. Results and discussion

3.1. Molecular characterization

Scheme 1 presents the illustration of the entire synthetic process from the monomers to blend and copolymers syntheses. The chemical structure of the synthesized copolymers, with the general formula P(BS-*b*-PeF)$_x$, is reported in Fig. 1. From the chemical point of view, it should be noted that the two repeating units differ both for the acid and glycol subunits: succinic moiety being linear and aliphatic whereas furan

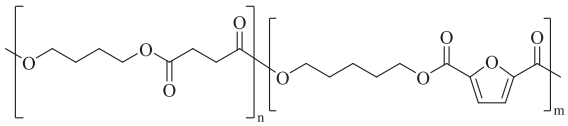

Fig. 1. General chemical structure of P(BS-*b*-PeF)$_x$ copolymers.

moiety containing an aromatic cyclic five-membered ring. GPC measurements confirm that both homopolymers and copolymers exhibit high and comparable molecular weights (Table 1), suggesting optimized synthesis conditions were achieved along with effective control over polymerization.

The chemical structure, composition and architecture of all polyesters were investigated through ^{1}H NMR and ^{13}C NMR spectroscopy. In all cases, the spectra were found to be consistent with the expected structures. The ^{1}H NMR spectrum of PBS shows the following resonance peaks: δ = 1.71 (m, 4H) corresponding to the aliphatic protons of butylene subunit in β position to the —COO— group; δ = 2.62 (s, 4H) relative to the aliphatic protons of succinic subunit and δ = 4.11 (t, 4H) relative to the aliphatic protons of butylene subunit in α position to the —COO— group (Fig. S1). The ^{1}H NMR spectrum of PPeF shows the following signals: δ = 1.55 (m, 2H) due to aliphatic protons on C_3 of pentamethylene subunit; δ = 1.84 (m, 4H) corresponding to aliphatic protons on C_2 of pentamethylene subunit; δ = 4.35 (t, 4H) ascribable to aliphatic protons of pentamethylene subunit in α position to —COO— group and δ = 7.19 (s, 2H) relative to aromatic protons of the furan ring (Fig. S2). In Fig. 2, the ^{1}H NMR spectrum of PBS/PPeF blend is shown together with peak assignment. As one can see, the PBS/PPeF spectrum is the mere sum of the parent homopolymers. Blend composition was calculated from the normalized areas of the resonance peak ***6*** (4.11 ppm) and ***2*** (4.35 ppm) corresponding to the —OCH_2- groups of butylene and pentamethylene subunits, respectively (Fig. 2) [30]. From

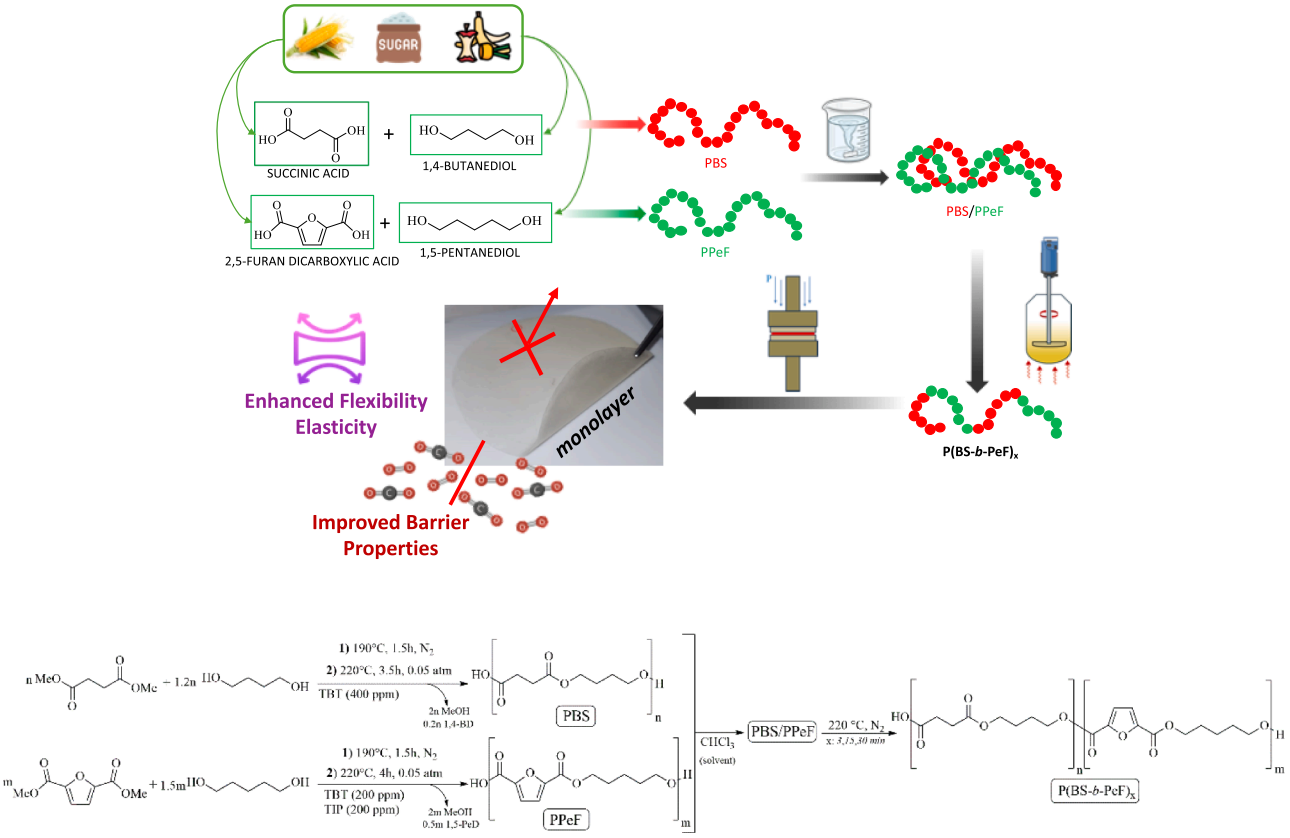

Scheme 1. Schematic representation of the overall work (top); PBS and PPeF syntheses, PBS/PPeF physical blend preparation and reactive blending to obtain the P(BS-*b*-PeF)$_x$ copolymers (bottom).

Table 1
Molecular characterization data of PBS, PPeF and P(BS-*b*-PeF)$_x$ copolymers.

Sample	PBS mol% ^{1}H NMR	PBS wt% ^{1}H NMR	M_n g/mol	D	L_{BS}	L_{BF}	L_{PeF}	L_{PeS}	*b*
PBS	100	100	49,100 ±200	2.1 ±0.07	–	–	–	–	–
P(BS-*b*-PeF)$_3$	56 ± 0.5	50 ± 0.5	39,800 ±200	2.2 ±0.07	26 ±0.5	–	18 ±0.3	–	0.08 ±0.01
P(BS-*b*-PeF)$_{15}$	56 ± 0.5	50 ± 0.5	43,200 ±200	2.1 ±0.07	10 ±0.3	–	8.5 ±0.3	–	0.20 ±0.01
P(BS-*b*-PeF)$_{30}$	56 ± 0.5	50 ± 0.5	40,500 ±200	2.1 ±0.07	5 ±0.1	1.60 ±0.07	3 ±0.1	1.37 ±0.1	1.9 ±0.01
PPeF	0	0	37,800 ±200	2.2 ±0.07	–	–	–	–	–

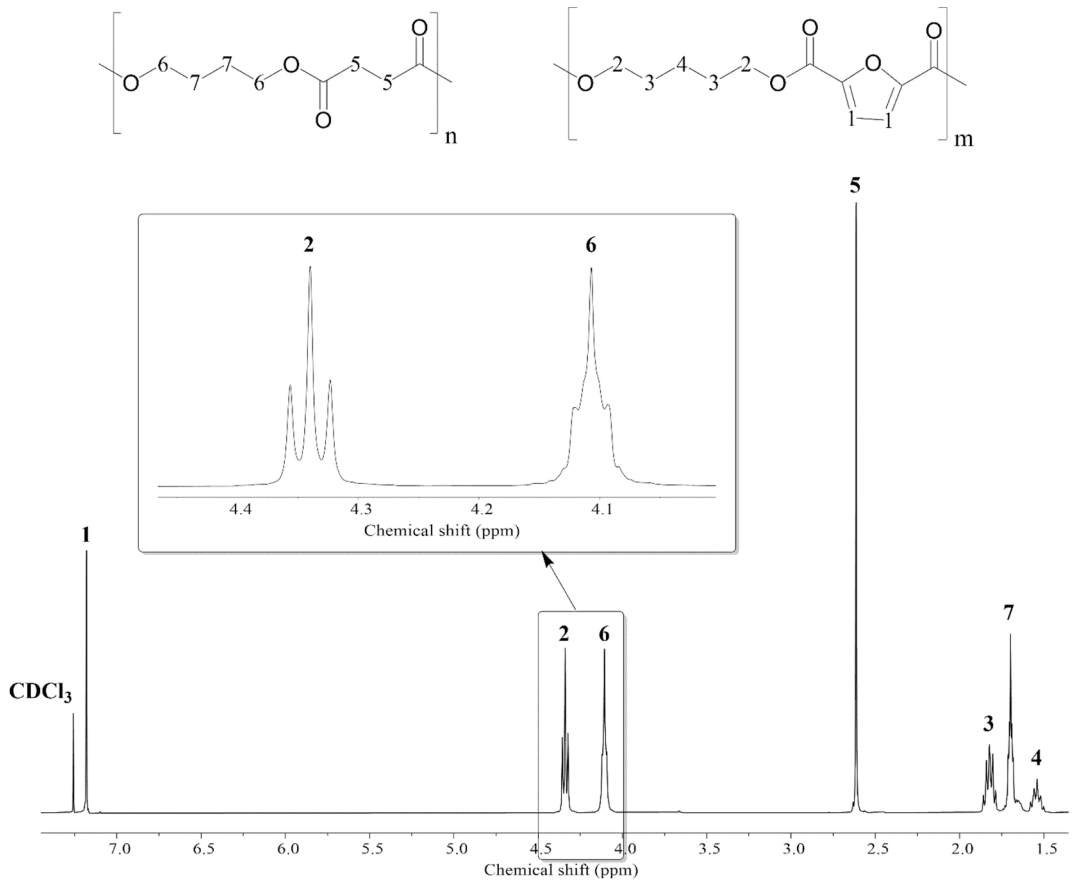

Fig. 2. ^{1}H NMR spectrum of PBS/PPeF blend with peak assignment and relative enlargement of the spectral region between 3.90 and 4.60 ppm.

the data reported in Table 1, it can be seen that the actual composition of the blend, as a consequence of the copolymers, corresponds to the feed one.

Block length, an important feature in determining the final properties of the copolymers, was investigated following the structural changes occurring in the blend, mixed at high temperature and in the presence of the catalyst, as a function of mixing time. Fig. 3 shows the ^{13}C NMR spectrum of P(BS-*b*-PeF)$_3$ copolymer with the peak's assignments. The ***5***, ***6***, ***8*** and ***10*** peaks (between 20–30 ppm) are relative to the aliphatic carbon atoms of pentamethylene, butylene and succinic subunits. The ***2*** and ***3*** peaks (at 146 and 118 ppm, respectively) are proper for the aromatic C atoms of the furan cycle. The ***1*** and ***7*** peaks correspond to the carbon atoms of the C═O groups of the succinic and furan moieties. Lastly, ***4*** and ***9*** peaks can be attributed to —OCH_2— of pentamethylene and butylene subunits, respectively. At the first stages, when the two homopolymers are not chemically linked, just the signals of —OCH_2— carbon atoms of the S-B-S and F-Pe-F triads can be detected: ***9*** and ***4***, respectively (Fig. 3). During copolymerization, because of the transesterification reactions, mixed triads identified as S-B-F and F-Pe-S (at short mixing times) and completely exchanged triads referred to as F-B-F and S-Pe-S (for very long mixing), are formed. This is the reason why, near the peaks due to the initial S-B-S and F-Pe-F triads, other six signals start growing: $\boldsymbol{4^1}$, $\boldsymbol{4^2}$, $\boldsymbol{9^1}$ and $\boldsymbol{9^2}$ peaks related to the mixed S-B-F and F-Pe-S triads, and ***4**** and ***9**** ones corresponding to the new F-B-F and S-Pe-S triads (enlargement in Fig. 3). Thus, from the relative intensities of —OCH_2— carbon atoms in the region between 63.9 and 65.5 ppm of ^{13}C NMR spectra (Fig. 3), it was possible to determine the block length and, consequently, the degree of randomness (*b*). It must be underlined that *b* is 0 for the neat physical blend of the homopolymers, i.e. no transesterification reactions took place, meaning just homopolymeric butylene succinate (—BS—) and pentamethylene furanoate (—PeF—) sequences are present in the material. Values of $b < 1$ indicate

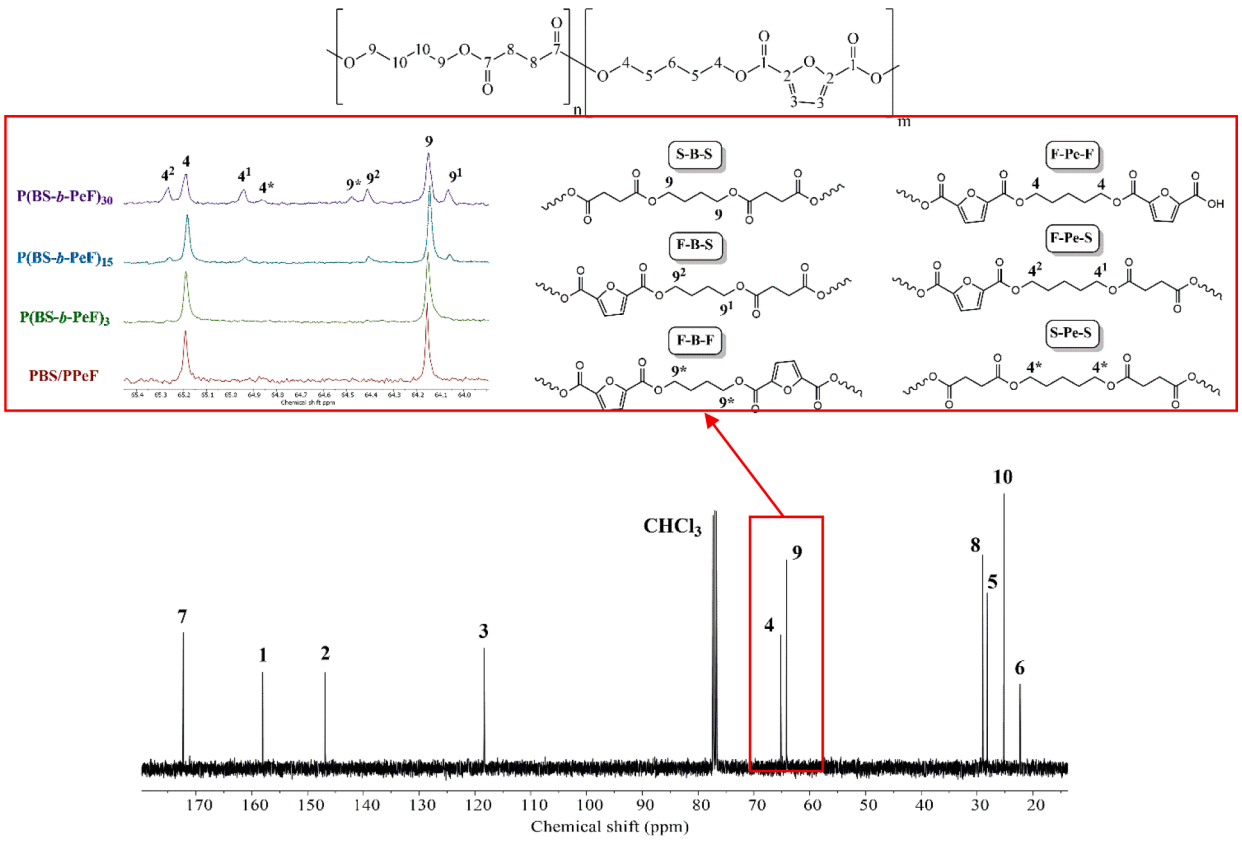

Fig. 3. ^{13}C NMR spectrum of P(BS-*b*-PeF)$_3$ with peak assignment. Enlargement of the spectral region between 63.9 and 65.5 ppm for the physical blend and the copolymers, together with a schematic representation of the possible triads present in the copolymers.

transesterification started but the copolymer units still tend to cluster in homogeneous —BS— and —PeF— sequences. When *b* is equal to 1, butylene furanoate (—BF—) and pentamethylene succinate (—PeS—) moieties start forming. A value of *b* greater than 1 indicates the amount —BF— and —PeS- sequences tends to the initial homopolymeric —BS— and —PeF- ones. *b* equal to 2 indicates a statistical distribution: initial S-B-S and F-Pe-F triads and exchanged F-B-F and S-Pe-S triads are equally probable, given the same composition of the initial homopolymers [31].

The degree of randomness (*b*) has been calculated as follows:

$$\boldsymbol{b} = P_{S-B-F} + P_{F-B-S} + P_{F-Pe-S} + P_{S-Pe-F}$$

where, $P_{S\text{-}B\text{-}F}$ and $P_{F\text{-}B\text{-}S}$ can be defined as the probability of finding a mixed triad S-B-F (or F-B-S) that interrupts a sequence of S-B-S (or F-B-F) triads. Similarly, $P_{F\text{-}Pe\text{-}S}$ and $P_{S\text{-}Pe\text{-}F}$ can be defined as the probability of finding a mixed triad F-Pe-S (or S-Pe-F) that interrupts a sequence of F-Pe-F (or S-Pe-S) triads. The probabilities are calculated as follows:

$$P_{S-B-F} = \frac{(I_{S-B-F} + I_{F-B-S})/2}{[(I_{S-B-F} + I_{F-B-S})/2] + I_{(S-B-S)}} P_{F-B-S} = \frac{(I_{S-B-F} + I_{F-B-S})/2}{[(I_{S-B-F} + I_{F-B-S})/2] + I_{(F-B-F)}}$$

$$P_{F-Pe-S} = \frac{(I_{(F-Pe-S)} + I_{(S-Pe-F)})/2}{[(I_{(F-Pe-S)} + I_{(S-Pe-F)})/2] + I_{(F-Pe-F)}} P_{S-Pe-F} = \frac{(I_{(F-Pe-S)} + I_{(S-Pe-F)})/2}{[(I_{(F-Pe-S)} + I_{(S-Pe-F)})/2] + I_{(S-Pe-S)}}$$

where $I_{S-B-S}, I_{S-B-F}, I_{F-B-S}, I_{F-B-F}$ represent the integrated intensities of the resonance signals: ***9***, ***9^1***, ***9^2*** and ***9****, respectively (Fig. 3). While $I_{F-Pe-F}, I_{F-Pe-S}, I_{S-Pe-F}, I_{S-Pe-S}$ correspond to integrated intensities of resonance signals: ***4***, ***4^1***, ***4^2*** and ***4****, respectively. The calculated probabilities allow to determine the block lengths. In detail, $\mathbf{L}_{BS}$ denotes the length of the −BS- blocks, while $\mathbf{L}_{BF}$ represents the length of the −BF- sequences. $\mathbf{L}_{PeF}$ refers to the length of the −PeF- blocks, while $\mathbf{L}_{PeS}$ represents the length of the −PeS- sequences. The calculation is shown below:

$$L_{BS} = \frac{1}{P_{S-B-F}} \quad L_{BF} = \frac{1}{P_{F-B-S}}$$

$$L_{PeF} = \frac{1}{P_{F-Pe-S}} \quad L_{PeS} = \frac{1}{P_{S-Pe-F}}$$

The average length of the sequences and the degree of randomness calculated for each copolymer are reported in Table 1. The results show that the higher the mixing time the higher the degree of randomness. As transesterification reactions took place, $\mathbf{L}_{BS}$ and $\mathbf{L}_{PeF}$ decreased, while the values of $\mathbf{L}_{BF}$ and $\mathbf{L}_{PeS}$ increased. As a matter of fact, P(BS-*b*-PeF)$_3$ copolymer shows the highest $\mathbf{L}_{BS}$ and $\mathbf{L}_{PeF}$ data, indicating mainly −BS- and −PeF- sequences are present in the sample. For P(BS-*b*-PeF)$_{15}$ copolymer, obtained at 15 min of mixing time: i) the ***4^1***, ***4^2*** and ***9^1***, ***9^2*** peaks start arising, indicating the formation of S-B-F and F-Pe-S triads that break the −BS- and −PeF- segments; ii) the ***4**** and ***9**** peaks are indistinguishable from the background noise, making it impossible to calculate their integrals for $\mathbf{L}_{BF}$ and $\mathbf{L}_{PeS}$ determination. In this case, one can assume −BF- and −PeS- sequences are still negligible. As reaction time further increases, ***4**** and ***9**** peaks show up indicating −BF- and −PeS- sequences are forming. Finally, it is possible to assess that the experimental conditions used allowed the preparation of a physical blend of the two homopolymers (PBS/PPeF) and a set of different block copolymers, whose −BS− and −PeF− block lengths decrease with mixing time.

3.2. Thermal and structural characterization

Thermal stability was evaluated through TGA analysis performed under dry nitrogen flow. The thermal degradation curves describing the evolution of the percentage gravimetric weight vs temperature are represented in Fig. S3. The corresponding data of temperature of initial decomposition (T_{onset}) and temperature of maximum degradation rate (T_{max}) are listed in Table 2. The thermal decomposition of PBS homopolymer occurs in a single narrow step, an outcome that is common for linear PBS as reported by Han et al. [32]. When PPeF homopolymer is subjected to heating in an inert atmosphere, it undergoes a process of thermal degradation within a specific temperature range which leads to 100 % weight loss [24]. PBS and PPeF homopolymers are the most thermally stable showing T_{onset} higher than 360 °C and T_{max} above 390 °C. Upon the comparison of TGA results of parent homopolymers with the corresponding blend and copolymers, it can be concluded that physical and chemical blending of PBS with PPeF do not significantly affect thermal stability, guaranteeing a wide processing window even for the blend and copolymers.

The polymeric films obtained through compression moulding were stored at room temperature for 10 days, before further characterization, to achieve equilibrium crystallinity. Subsequently, the thermal behaviour of the films was analyzed using Differential Scanning Calorimetry (DSC). The data related to the observed transitions are collected in Table 2. The I and II scan corresponding traces are reported in Fig. 4A and B. The two homopolymers exhibit significantly different thermal characteristics. PBS is semicrystalline, with a glass transition temperature (T_g) around –32 °C and a melting temperature (T_m) at 113 °C. The melting behaviour of PBS is quite complex. In the literature, it is reported PBS heating calorimetric curves can vary significantly based on the polymer's molecular weight, thermal history and the thermal gradient used [32,33]. The PBS we synthesized exhibits a single melting peak, preceded by partial crystallization at 90 °C (exothermic peak) which, as reported by Righetti et al. [34], could result from the formation of a second crystalline population, developing under heating, with the same morphology but different thicknesses, melting at the same temperature as the original one. In the first scan of PBS, an annealing peak can also be observed at around 40 °C.

PPeF film is an amorphous material with a T_g of 17 °C. However, the film stored at room temperature for two months (dotted line in Fig. 4A) displays a small and wide endothermic peak around 52 °C due to a slow crystallization process that occurred during storage. In the second scan (Fig. 4B), both PBS and PPeF show a behaviour similar to the one observed in the first scan, confirming for PBS the high crystallization rate as opposed to the modest ability of PPeF macromolecules to reorganize in crystalline structures.

For PBS/PPeF film, the calorimetric curve shows a melting peak at 113 °C, associated with the PBS fraction, in both the first and second scans. This result indicates PBS fraction retains its excellent crystallization ability, even in the blend. As neat PBS, PBS/PPeF physical blend also exhibits an exothermic crystallization peak just before T_m (at 93 °C in the first scan and 101 °C in the second scan). Additionally, an annealing peak is observed at around 40 °C in the first scan. An inflexion point at 12 °C due to the T_g of the PPeF fraction can be also detected; the T_g of the PBS fraction is not distinguishable in the trace. The lack of significant shifts in the temperatures associated with the glass transition and melting phenomena indicates that PBS and PPeF are not miscible in the physical blend. SEM analysis and mechanical property studies will further determine whether the two fractions are at least compatible.

Copolymers exhibit different thermal behaviours depending on the block length. P(BS-*b*-PeF)$_3$ copolymer shows a T_g of −4 °C, intermediate between the two homopolymers, while T_m is around 107 °C both before and after rapid cooling from the melt. The decrease in T_m compared to PBS aligns with a reduction in homopolymer −BS- sequences. As for the PBS/PPeF blend and PBS homopolymer, rapid cooling does not quench the material, as it still shows a melting peak in the second scan. However, no crystallization occurs before the endothermic peak. In the first scan, also for P(BS-*b*-PeF)$_3$, a second endothermic peak appears around 40 °C. For P(BS-*b*-PeF)$_{15}$ copolymer, T_g further decreases, with the glass transition step observed at −19 °C. The melting peak also occurs at a lower temperature, 79 °C, and is only visible in the first scan, indicating a reduced crystallization capability of the melt, both under cooling and heating. Again, a second endotherm is observed at 42 °C in the first scan. P(BS-*b*-PeF)$_{30}$ copolymer presents a T_g of −16 °C, and a quite large endothermic peak at 43 °C in the first scan, while in the second scan, it just undergoes glass to rubber transition. Generally, medium to short block copolymers do not show any endothermic peaks in the second scan, indicating that rapid cooling of the melt effectively quenched the material that, due to the lowering in block length, is not more able to fold in crystalline lattices in the second scan heating.

To summarise, as the block length decreases and the sequence distribution becomes more statistical, miscibility between PBS and PPeF homopolyesters increases. Consequently, T_g moves to values intermediate between those of the parent homopolymers. As a concern, the main melting endotherm, both melting temperature (T_{m2}) and enthalpy (ΔH_{m2}-ΔH_{cc}) decreases with shorter block lengths (see Fig. 4C), indicating that the PBS fraction crystallizes at a lower extent forming fewer and less perfect crystals. Conversely, the enthalpy of the endothermic signal around 40 °C progressively increases, while maintaining the same T_{m1} value (Fig. 4C). For PBS homopolymer, the endothermic transition at 40 °C is attributed to the isotropization of imperfect crystal formed during storage at room temperature (annealing). This signal is also observed in the copolymers at the same temperature. In the copolymers, as proposed for other polyesters containing mesogenic groups, its origin could be linked to the isotropization of a mesophase characterized by lower spatial order compared to a tridimensional crystalline domain [35]. Interestingly, the intensity of the peak around 40 °C (ΔH_{m1}) increases as the block length decreases, suggesting an increase in

Table 2
Thermal characterization data of PBS, PPeF, PB/PPeF and P(BS-*b*-PeF) copolymers. The relative degree of crystallinity (X_c) calculated from WAXS analysis is also reported. The error on the calorimetric data is about 2%. For the sake of clarity, it is not reported in the table.

Sample	I SCAN				II SCAN								
	T_{cc} (°C)	ΔH_{cc} (J/g)	$T_{m1\text{-}2}$ (°C)	$\Delta H_{m1\text{-}2}$ (J/g)	T_g (°C)	ΔC_p (J/g*C)	T_{cc} (°C)	ΔH_{cc} (J/g)	T_m (°C)	ΔH_m (J/g)	T_{onset} (°C)	T_{max} (°C)	X_c (%)
PBS	90	11.2	40 113	2.2 60.2	–32	0.18	96	7.8	113	60.5	365	394	47 ± 5
PPeF	–	–	–	–	17	0.39	–	–	–	–	370	392	–
PBS/PPeF	93	6.3	40 113	1.2 34.2	12	0.26	101	2.0	113	27.7	355	378	26 ± 3
P(BS-*b*-PeF)$_3$	–	–	43 106	5.5 32.7	−4	0.42	–	–	107	34.7	362	397	29 ± 3
P(BS-*b*-PeF)$_{15}$	–	–	42 79	8.8 16.4	−19	0.45	–	–	–	–	368	394	27 ± 3
P(BS-*b*-PeF)$_{30}$	–	–	43	27.2	−16	0.49	–	–	–	–	355	387	21 ± 2

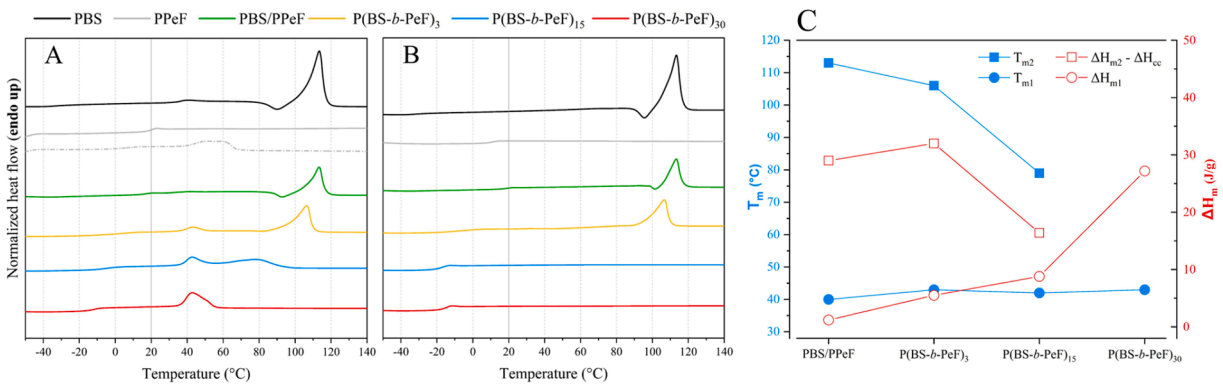

Fig. 4. DSC curves of homopolymers, blend and copolymers:(A) I scan and (B) II scan. Semicrystalline PPeF film (dotted line) is also included for the sake of comparison. (C) Melting temperatures T_{m1} and T_{m2} (blue), and corresponding enthalpies (red; ΔH_{m1} and ΔH_{m2}- ΔH_{cc}) for blend and copolymers.

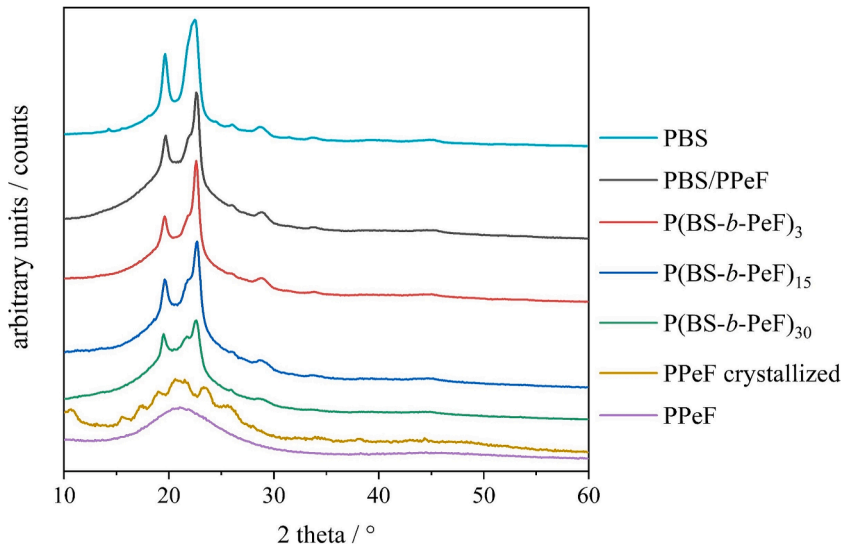

Fig. 5. Diffraction patterns of homopolymers, blend and copolymers compression moulded films. Crystallized PPeF film is also included for the sake of comparison.

mesophase regions at the expense of crystalline ones.

To corroborate calorimetric results and to investigate the microstructure of the samples, wide-angle X-ray scattering analysis on the compression moulded films was carried out. WAXS patterns are shown in Fig. 5. The relative degree of crystallinity (X_c) is reported in Table 2. PBS and all the derived PBS samples present the common diffractogram of a semicrystalline material comprehending the amorphous halo, related to the amorphous phase, and a series of reflections, in particular, the main ones at 19.5 and 22.5 θ related to PBS crystal phase corresponding to (020) and (110) plane, respectively [36]. PPeF homopolymer presents an amorphous halo due to the presence of only an amorphous portion as stated by DSC, confirming that the polymer did not have sufficient time to develop crystalline microstructures. With the introduction of PPeF in the blend there is an associated rise in the area under the bell-shaped background line, which is directly proportional to the fraction of the amorphous phase. This phenomenon is accompanied by a reduction in reflection intensities, caused by the decrease of the ordered phase, ultimately leading to a decrease in the degree of crystallinity. As previously demonstrated by DSC experiments, this trend is consistent and indicative of a reduction in crystallinity degree attributable to the lower amount of PBS fraction in the blend. In the copolymers with higher block lengths, the degree of crystallinity seems to remain almost constant. In the case of P(BS-*b*-PeF)$_{30}$ copolymer, there is a consistent reduction of X_c as a consequence of the reduced crystallization capability of shorter −BS- segments.

Comparing the WAXS pattern of all the PBS-based materials with the diffractogram of crystallized PPeF (stored for several months at room temperature), one can see no PPeF crystal reflections are present. This result suggests the crystalline lattice of the blend and copolymers only comes from −BS- segments. Combining this evidence with DSC analysis, it is possible to conclude that the endothermic peaks present in the DSC curves are not ascribable to PPeF crystal domains.

3.3. Morphological characterization

In the literature, SEM analysis is often used to check possible phase segregation in polymeric blends. Previous works have reported about PLA/PPeF blends showing the two homopolymers are not compatible segregating each other [37]. Fig. 6 reports the SEM images, at different magnifications, acquired on the cryofracture section of PBS/PPeF blend (A) and P(BS-*b*-PeF)$_{15}$ (B) copolymer films. Based on SEM analysis, the PBS/PPeF blend shows a certain degree of compatibility between the two homopolymers: just small cavities and protrusions can be observed, nevertheless the surface is quite smooth and homogeneous. At high magnification, phase separation can be detected, in line with the DSC results that had highlighted the two parent homopolymers are not miscible. More in detail, one can observe a continuous matrix (probably related to PBS) containing small microdomains (likely ascribable to PPeF) with circular morphology (highlighted by red arrows in Fig. 6A right panel). The absence of fractures, discontinuities and the

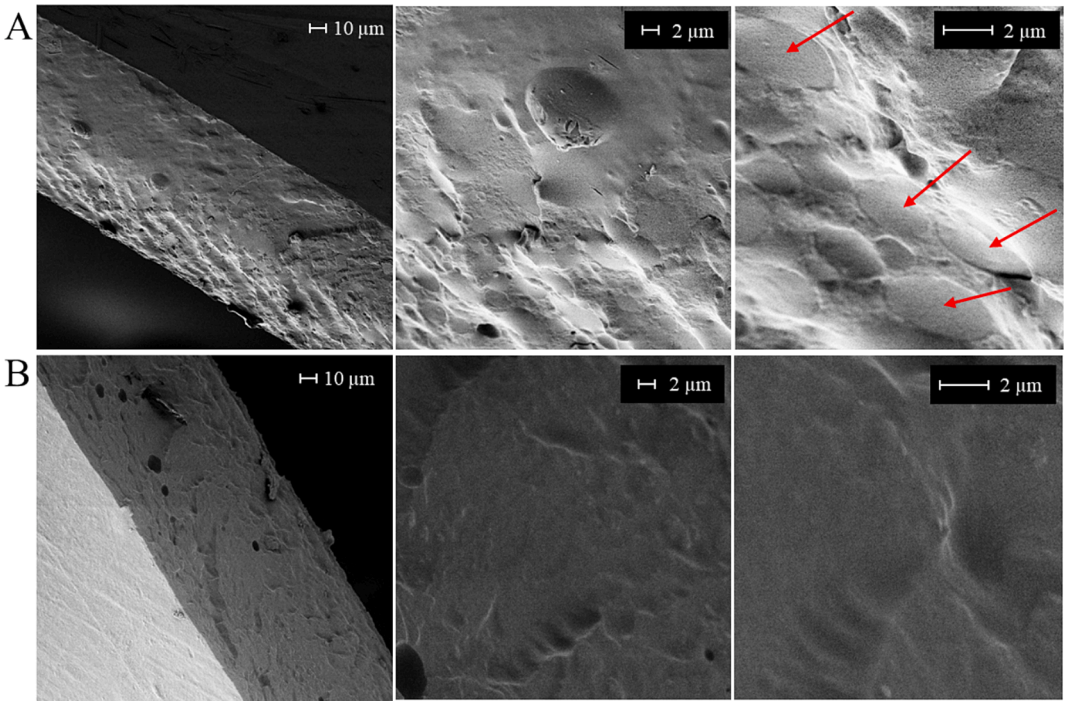

Fig. 6. SEM images of the cryo-fractured cross-section of PBS/PPeF (A) and P(BS-*b*-PeF)$_{15}$ (B) films.

homogenous distribution of one phase in the other one suggest a good compatibility of PBS and PPeF components. Phase separation is not observed in copolymers, as reported for P(BS-*b*-PeF)$_{15}$ in Fig. 6B. Thus, copolymerization has allowed for further enhancement of the compatibility of the two homopolymers by eliminating the interface between the continuous matrix and dispersed microdomains.

3.4. Mechanical characterization

Tensile tests were performed on the film of all polymer samples. The stress–strain curves are represented in Fig. 7. The experimental values of

Table 3
Mechanical characterization data.

Polymer	*E* (MPa)	ε_b (%)	σ_b (MPa)
PBS	473 ± 28	219 ± 70	23 ± 2
PPeF	4.2 ± 0.5	1166 ± 95	0.8 ± 0.2
PBS/PPeF	160 ± 23	400 ± 114	15 ± 2
P(BS-*b*-PeF)$_3$	103 ± 5	1130 ± 148	18 ± 4
P(BS-*b*-PeF)$_{15}$	87 ± 7	1132 ± 123	13 ± 1
P(BS-*b*-PeF)$_{30}$	32 ± 2	1074 ± 234	4 ± 1

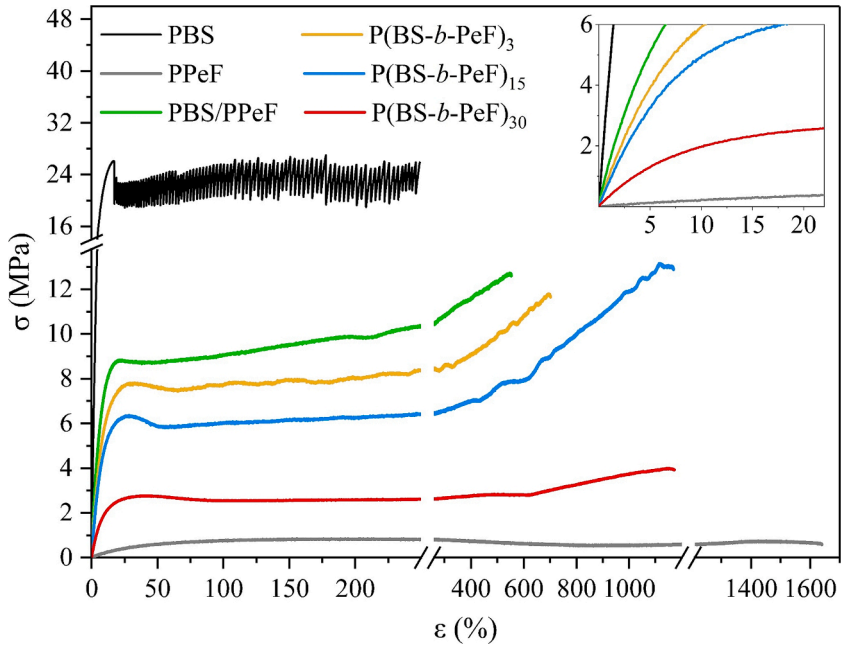

Fig. 7. Stress–strain curves of the samples. In the insert: magnification of the curves at low strain values.

elastic modulus (E), stress at break (σ_b) and elongation at break (ε_b) are collected in Table 3.

PBS homopolymer exhibits a relatively high elastic modulus, in line with its semicrystalline nature. Following the initial elastic region, after the yield point, there is a discontinuous yielding with a "zig-zag" pattern. The material displays a rather high elongation, and once it reaches the break, it does not show shape recovery. The "zig-zag" pattern in the curve reflects in the final morphology of the specimens, which display a series of stripes perpendicular to the stretching direction. This inhomogeneous plastic deformation has been observed in polycrystalline materials such as metals and semicrystalline polymers [38,39]: during stretching, the slipping of crystalline planes can produce marks of deformation on the surface and stress oscillation in the stress–strain curve of semicrystalline polymers, as in the case of PBS [40,41]. PPeF homopolymer, as evidenced by DSC analysis, is in the rubbery amorphous state at room temperature. It is characterized by low elastic modulus, high elongation at break, and the absence of yield point. Even if not crosslinked, PPeF specimens exhibit high shape recovery after fracture. This surprising response has been attributed to the presence of a 2D-ordered phase resulting from interchain pseudo-hydrogen bonds as well as π- π interactions, which are further strengthened during the film formation process through compression moulding [24]. It can be noted that PBS/PPeF exhibits intermediate values of elastic modulus, elongation and stress at break compared to the homopolymers composing it. That further confirms what was observed in the SEM images: the two homopolymers PBS and PPeF in the physical blend display a certain degree of compatibility, being well dispersed by each other [42,43]. Regarding the copolymers, they all are characterized by high elongation at break, however, there is a decrease in both elastic modulus and stress at break proportional to the decrease in block length that, in turn, determines crystallinity degree drop. As the copolymers move towards a statistical distribution of repeating units, their mechanical properties gradually resemble those of a viscoelastic material. Observing the stress–strain curves, it is noticeable that the copolymers do not exhibit a clear yield point, in particular in the case of P(BS-*b*-PeF)$_{30}$ copolymer. As for PPeF, it is not possible to distinguish between the elastic and plastic deformation zones, resembling an elastomer. This behaviour can be attributed to the presence of pseudo-hydrogen bonds acting as physical netpoints, as previously reported [24].

Cyclic tests were conducted to analyze the load-unload behaviour of copolymers. Three tests were performed at increasing strain levels: 5, 15 and 30 %. The resulting maximum elongation for each test considers the pre-tensioning of the dynamometer, thus resulting in a slightly lower value. The shape recovery was calculated based on the first cycle as shown below:

$$shape\,recovery(\%) = \frac{\text{LOADING } elongation\,\% - \text{UNLOADING } elongation\,\%}{\text{LOADING } elongation\,\%} *100$$

Hysteresis, on the other hand, was evaluated on the tenth cycle, of which the area has been calculated. The resulting data are summarized in Table 4. Fig. 8 reports the stress–strain curves resulting from the third experiment (30 % maximum elongation) conducted on P(BS-*b*-PeF)$_3$ copolymer.

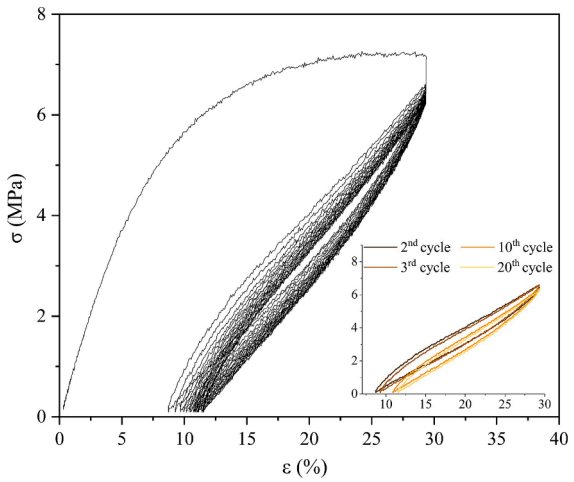

Fig. 8. Stress–strain curve obtained from the cyclic test of the sample P(BS-b-PeF)$_3$ at 30% of maximum elongation. Insert: 2nd, 3rd, 10th and 20th cycles.

Lower strains result in a slightly higher percentage of shape recovery for P(BS-*b*-PeF)$_3$ and P(BS-*b*-PeF)$_{15}$ copolymers. However, this trend is not observed for copolymer P(BS-*b*-PeF)$_{30}$, for which the shape recovery remains nearly constant regardless the strain applied. That suggests the higher elastomeric nature of the copolymer with shorter block lengths. As deformation increases, hysteresis naturally increases as well. With the same level of deformation, hysteresis decreases as the block length of copolymers decreases, indicating again an enhanced elastomeric behavior for shorter block copolymers.

3.5. Gas barrier analysis

The results of the permeability tests to oxygen and carbon dioxide,

Table 5
Values of GTR of O_2 and CO_2 collected at 23 °C and normalized for film thickness, and Barrier Improvement Factor (BIF) for O_2 and CO_2.

Polymer	Thickness (μm)	O_2 –*TR* (cm^3 cm/m^2 d atm)	CO_2-*TR* (cm^3 cm/m^2 d atm)	BIF O_2	BIF CO_2
PBS	*185*	0.695 ± 0.035	2.37 ± 0.1	–	–
PPeF	*150*	0.002 ± 0.0005	0.002 ± 0.0005	–	–
PBS/PPeF	*182*	0.637 ± 0.025	2.27 ± 0.1	1.09	1.04
P(BS-*b*-PeF)$_3$	*173*	0.351 ± 0.025	2.18 ± 0.05	1.98	1.08
P(BS-*b*-PeF)$_{15}$	*143*	0.090 ± 0.025	1.75 ± 0.05	7.76	1.35
P(BS-*b*-PeF)$_{30}$	*255*	0.150 ± 0.025	2.6 ± 0.1	4.64	0.92

Table 4
Cyclic tests data. The error on the data does not exceed 5%. For the sake of clarity, it is not reported in the table.

Polymer	Experiment 1			Experiment 2			Experiment 3		
	elongation (%)	**shape recovery** (%)	**hysteresis** (KJ/mm^3)	**elongation** (%)	**shape recovery** (%)	**hysteresis** (KJ/mm^3)	**elongation** (%)	**shape recovery** (%)	**hysteresis** (KJ/mm^3)
P(BS-*b*-PeF)$_3$	4.3	81.7	0.0080	14.4	75.6	0.0590	29.4	70.3	0.1144
P(BS-*b*-PeF)$_{15}$	3.4	81.4	0.0030	14.0	76.4	0.0407	29.1	73.5	0.0950
P(BS-*b*-PeF)$_{30}$	3.7	76.3	0.0017	13.2	71.8	0.0144	29.2	77.3	0.0465

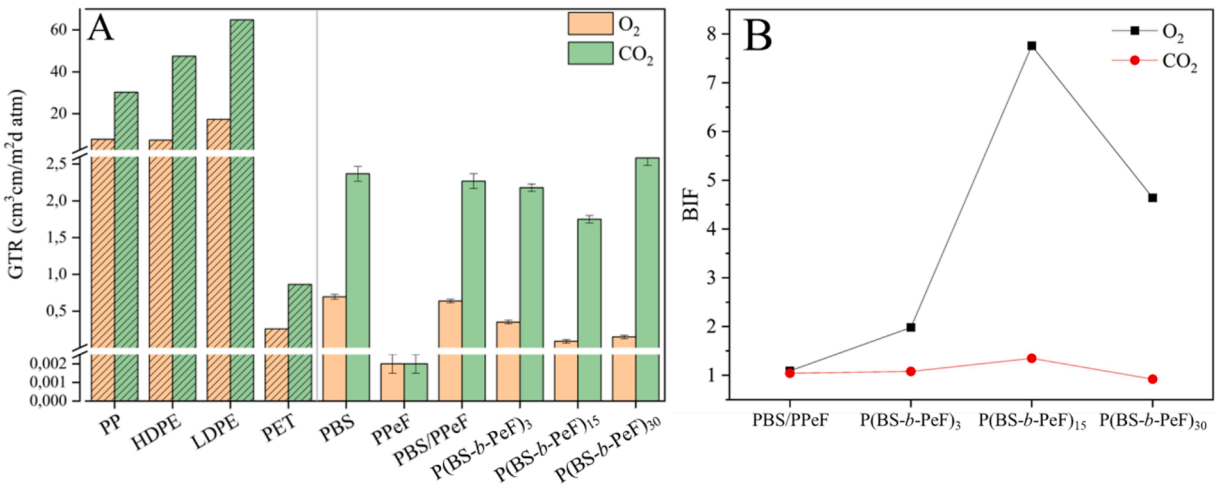

Fig. 9. A) O_2 and CO_2 transmission rates at 23 °C in a dry (0 % RH) atmosphere for PBS and PPeF homopolymer, PBS/PPeF blend and P(BS-b-PeF)$_x$ copolymers and food packaging commodities [44]; B) Barrier Improvement Factor (BIF) for O_2 and CO_2 of PBS/PPeF blend and P(BS-b-PeF)$_x$ copolymers films with respect to neat PBS.

for PBS and PPeF homopolymers, PBS/PPeF blend and P(BS-*b*-PeF)$_x$ copolymers are reported in the following as Gas Transmission Rate (GTR) values (Table 5) and compared in Fig. 9 with some commodities widely used in food packaging industry: poly(propylene) (PP), high-density poly(ethylene) (HDPE), low-density poly(ethylene) and poly (ethylene terephthalate) (PET) [44]. As reported in the literature and confirmed in this study, PPeF film shows an outstanding gas barrier property, due to the presence of a mesophase, making it resemble a liquid-crystalline polymer. The film manufacturing process through compression moulding promotes the formation of an ordered structure, with the furan ring acting as a mesogenic group [24]. PBS does not reach GTR values of PPeF, yet it still exhibits superior barrier properties compared to the most used polyolefins in food-packaging. PBS/PPeF blend shows permeability very similar to PBS. Copolymers reveal a decrease in both O_2-TR and CO_2-TR values, meaning a gas barrier capability improvement with respect to PBS, as the block length decreases, reaching a minimum for P(BS-*b*-PeF)$_{15}$ copolymer. A further shortening of blocks did not produce additional GTR values decrease. Specifically, P(BS-*b*-PeF)$_{30}$ exhibits increased permeability compared to the copolymers with long to medium-length blocks. The results obtained suggest the formation of mesogenic microstructure, particularly effective in locking the gas passage through the polymer film, is favoured in P(BS-*b*-PeF)$_{15}$ copolymer with respect to tridimensional crystal phase, in line with the DSC data: being the isotropization enthalpy (ΔH_{m1}) higher and melting heat (ΔH_{m2}- ΔH_{cc}) lower with respect to the blend and the longer block copolymers.

In general, among all the films under study, the improvement in gas barrier capability is more pronounced for oxygen, for which the permeability decreases by almost one order of magnitude with respect to PBS homopolymer, while the CO_2-TR value decreases by 25 % in the best case (P(BS-*b*-PeF)$_{15}$). In this respect, the Barrier Improvement Factor (BIF) for O_2 and CO_2 of PBS/PPeF blend and P(BS-*b*-PeF)$_x$ copolymers films with respect to neat PBS, has been calculated and reported in Fig. 9 and Table 5. The BIF values for CO_2 and O_2 show a quite different trend:

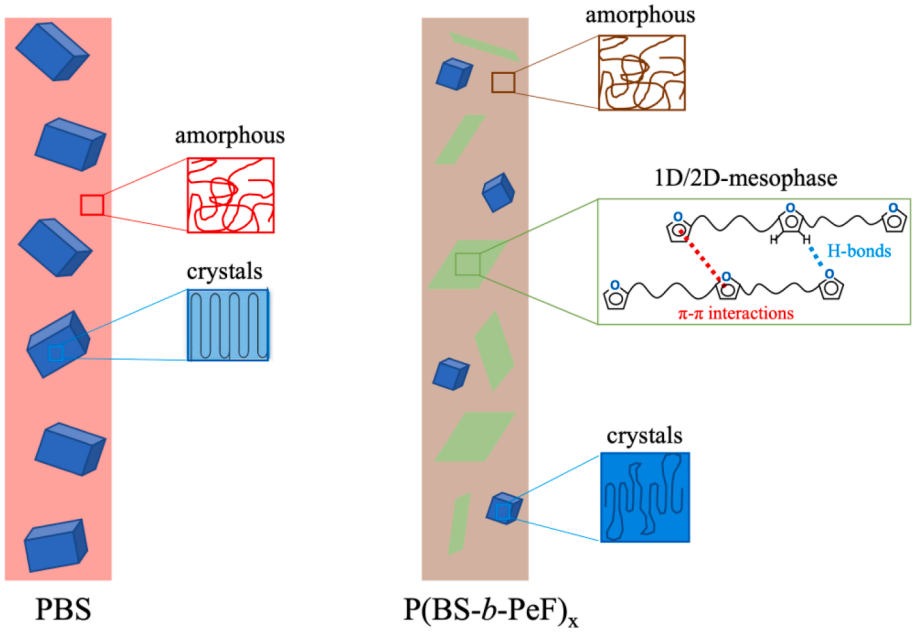

Scheme 2. Schematic representation of the hypothesized macromolecular arrangement in PBS and P(BS-b-PeF)$_x$ copolymers, on the basis of previous results on PPeF [24].

CO_2 BIF being slightly higher than 1 and comparable for P(BS-*b*-PeF)$_x$ copolymers except P(BS-*b*-PeF)$_{30}$ for which it is even slightly less than 1. In the case of O_2, BIF values besides being quite higher than 1, are also tunable by playing with the block length. In particular, it can be enhanced by shortening the −BS- (and −PeF-) sequences in the macromolecular chains, up to the P(BS-*b*-PeF)$_{15}$ sample. An overall outlook reveals the possibility of *ad-hoc* balancing O_2 permeability keeping CO_2 transmission constant.

Scheme 2 describes the possible macromolecular arrangement established in PBS homopolymer (left side) and in P(BS-*b*-PeF)$_x$ copolymers (right side). In the neat PBS, the presence of crystalline as well as amorphous regions can be hypothesized, as suggested by DSC and WAXS analyses. In the copolymers, a third fraction, 1D/2D-mesophase can be also supposed, this last arising from the furan rings capable of establishing interchain π-π and H-bond like interactions. Mesophase arrangements are responsible both for the elastic behavior and the better gas blocking ability. Mesophase develops at the expense of the crystalline regions, which, in the copolymers are composed of fewer and less perfect crystals as confirmed by DSC and WAXS results. Mesophase arrangements are responsible both for the elastic behaviour and the better gas blocking ability of the copolymers.

4. Conclusions

Innovative fully biobased aliphatic–aromatic polyesters have been synthesized starting from poly(butylene succinate) (PBS) and poly (pentamethylene 2,5-furanoate) (PPeF), previously prepared by melt polycondensation, through both physical and reactive blending, the former being an easy and a cost-effective process and the latter a fast and solvent-free strategy.

Even if not miscible, PBS and PPeF showed good compatibility already in the PBS/PPeF physical blend, as confirmed by the good matrices dispersion evidenced by SEM analysis, which reflects into enhanced flexibility and elongation while preserving O_2 and CO_2 barrier. NMR data, along with DSC and XRD results, provide evidence that reactive blending yields block copolymers. Notably, the block length together with the crystallizing ability, ascribable to −BS- segments, decreases as the mixing time increases. Transesterification reactions, occurring during reactive blending, butylene succinate moieties to connect to pentamethylene furanoate units producing firstly block ($0 < b < 2$) and then random copolymers ($b \approx 2$). That further favours PBS and PPeF compatibility as demonstrated by the greater homogeneity and regularity, i.e. no phase separation, of the copolymers, both on the surface and in bulk, evidenced by SEM morphological study. In particular, P(BS-*b*-PeF)$_{15}$ copolymer has been selected as the material potentially most appropriate for the final purpose due to the optimal balance between mechanical response (from the enhanced flexibility and good strength to the elastomeric behaviour, as highlighted by tensile stress–strain and cyclic tests) and the best barrier properties within the series, comparable to PET and superior to polyolefin commodities.

Eco-design allowed the preparation of processable monolayer materials with higher impermeability to O_2 and CO_2, flexible and elastic, suitable for sustainable and flexible food packaging.

Mechanical elastomeric behaviour as well as the barrier ability improvement detected in the P(BS-*b*-PeF)$_x$ copolymers, could be associated with the formation of 1D/2D-ordered phases. We hypothesized this kind of arrangement could arise from the mesogenic furan rings determining the establishment of π-π interactions and H-bonds.

The system proposed turns out to be better than the commercial plastic materials such as PLA and PBAT. PLA is a biobased plastic known for its stiffness, as a matter of fact it is usually plasticized, and presents moderate gas barrier ability. On the other side, PBAT is flexible, but not elastic, and it is not fully biobased. The polymers proposed here are fully biobased, flexible/elastic and characterized by superior gas block capability.

The strategy employed, perfectly aligned with the principles of Green Chemistry, allowed the preparation of new materials with *ad-hoc* properties for the envisioned final application: monolayer flexible food packaging.

Due to the chemical and physical characteristics, the polyesters studied in the present work, following their use, can be evaluated both for recycling and composting.

CRediT authorship contribution statement

Mattia Manfroni: Writing – original draft, Methodology, Investigation, Formal analysis, Data curation. **Alessandro Coatti:** Writing – original draft, Investigation, Formal analysis, Data curation. **Michelina Soccio:** Writing – review & editing, Writing – original draft, Visualization, Validation, Supervision, Project administration, Conceptualization. **Valentina Siracusa:** Writing – review & editing, Validation, Supervision, Methodology, Investigation, Formal analysis, Data curation. **Elisa Boanini:** Writing – review & editing, Validation, Supervision, Methodology, Investigation, Formal analysis, Data curation. **Elisabetta Salatelli:** Writing – review & editing, Visualization, Supervision, Data curation. **Nadia Lotti:** Writing – review & editing, Validation, Supervision, Project administration, Methodology, Funding acquisition, Conceptualization.

Declaration of competing interest

The authors declare that they have no known competing financial interests or personal relationships that could have appeared to influence the work reported in this paper.

Acknowledgments

This publication is based upon work from Alma Idea 2022, Linea B2, CUP J33C22001420001, supported by University of Bologna.

Appendix A. Supplementary material

Supplementary data to this article can be found online at https://doi.org/10.1016/j.eurpolymj.2025.113728.

Data availability

Data will be made available on request.

References

[1] Plastics Europe AISBL, Plastic the facts 2023, 2023.
[2] G. Meral, Global Plastics Outlook - Policy Scenarios to 2060, n.d.
[3] R. Geyer, J.R. Jambeck, K.L. Law, Production, use, and fate of all plastics ever made, 2017. http://advances.sciencemag.org/.
[4] Hannah Ritchie, Veronika Samborska and Max Roser (2023) - "Plastic Pollution" Published online at OurWorldinData.org. Retrieved from: "https://ourworldindata.org/plastic-pollution" [Online Resource], (n.d.).
[5] S. RameshKumar, P. Shaiju, K.E. O'Connor, Bio-based and biodegradable polymers - State-of-the-art, challenges and emerging trends, Curr. Opin. Green Sustain. Chem. 21 (2020) 75–81, https://doi.org/10.1016/j.cogsc.2019.12.005.
[6] Single-use plastics, a roadmap for sustainability, United Nations Environment Programme, 2018.
[7] L.R. Gordon, Food Packaging. Principles and Practice, second ed., 2005.
[8] Directive (EU) 2018/ of the European Parliament and of the Council of 30 May 2018 amending Directive 1999/31/EC on the landfill of waste, 2018.
[9] C. Maes, W. Luyten, G. Herremans, R. Peeters, R. Carleer, M. Buntinx, Recent updates on the barrier properties of ethylene vinyl alcohol copolymer (EVOH): a review, Polym. Rev. 58 (2018) 209–246, https://doi.org/10.1080/15583724.2017.1394323.
[10] M.S. Kim, H. Chang, L. Zheng, Q. Yan, B.F. Pfleger, J. Klier, K. Nelson, E.L. W. Majumder, G.W. Huber, A review of biodegradable plastics: chemistry, applications, properties, and future research needs, Chem. Rev. 123 (2023) 9915–9939, https://doi.org/10.1021/acs.chemrev.2c00876.
[11] Global Production capacities of bioplastics 2023–2028, 2023. http://www.european-bioplastics.org/news/publica-.

[12] K.Y. Perera, A.K. Jaiswal, S. Jaiswal, Biopolymer-based sustainable food packaging materials: challenges, solutions, and applications, Foods 12 (2023), https://doi.org/10.3390/foods12122422.
[13] M. Barletta, C. Aversa, M. Ayyoob, A. Gisario, K. Hamad, M. Mehrpouya, H. Vahabi, Poly(butylene succinate) (PBS): materials, processing, and industrial applications, Prog. Polym. Sci. 132 (2022), https://doi.org/10.1016/j.progpolymsci.2022.101579.
[14] Q. Liu, X.M. Zhou, Syntheses and physical characterization of biodegradable poly (butylene succinate-co-butylene itaconate) copolymers, J. Macromol. Sci. Part A Pure Appl. Chem. 52 (2015) 745–751, https://doi.org/10.1080/10601325.2015.1063875.
[15] P. Ma, D.G. Hristova-Bogaerds, P.J. Lemstra, Y. Zhang, S. Wang, Toughening of PHBV/PBS and PHB/PBS blends via in situ compatibilization using dicumyl peroxide as a free-radical grafting initiator, Macromol. Mater. Eng. 297 (2012) 402–410, https://doi.org/10.1002/mame.201100224.
[16] S. Su, R. Kopitzky, S. Tolga, S. Kabasci, Polylactide (PLA) and its blends with poly (butylene succinate) (PBS): a brief review, Polymers (Basel) 11 (2019), https://doi.org/10.3390/polym11071193.
[17] J. Li, Z. Qiu, Fully biodegradable Poly(butylene succinate-co-1,2-decylene succinate)/Cellulose nanocrystals composites with significantly enhanced crystallization and mechanical property*, Polymer (Guildf) 252 (2022), https://doi.org/10.1016/j.polymer.2022.124946.
[18] J. Domínguez-Robles, E. Larrañeta, M.L. Fong, N.K. Martin, N.J. Irwin, P. Mutjé, Q. Tarrés, M. Delgado-Aguilar, Lignin/poly(butylene succinate) composites with antioxidant and antibacterial properties for potential biomedical applications, Int. J. Biol. Macromol. 145 (2020) 92–99, https://doi.org/10.1016/j.ijbiomac.2019.12.146.
[19] M.R. Nobile, A. Crocitti, M. Malinconico, G. Santagata, P. Cerruti, Preparation and characterization of polybutylene succinate (PBS) and polybutylene adipate-terephthalate (PBAT) biodegradable blends, in: AIP Conf Proc, American Institute of Physics Inc., 2018, https://doi.org/10.1063/1.5046042.
[20] B. Program, T. Werpy, G. Petersen, Top Value Added Chemicals from Biomass Volume I-Results of Screening for Potential Candidates from Sugars and Synthesis Gas Produced by the Staff at Pacific Northwest National Laboratory (PNNL) National Renewable Energy Laboratory (NREL) Office of Biomass Program (EERE) For the Office of the Energy Efficiency and Renewable Energy, n.d. http://www.osti.gov/bridge.
[21] S. Pandey, M.J. Dumont, V. Orsat, D. Rodrigue, Biobased 2,5-furandicarboxylic acid (FDCA) and its emerging copolyesters' properties for packaging applications, Eur. Polym. J. 160 (2021), https://doi.org/10.1016/j.eurpolymj.2021.110778.
[22] K. Nasr, A. Favrelle-Huret, R. Mincheva, G. Stoclet, M. Bria, J.M. Raquez, P. Zinck, The impact of diethyl furan-2,5-dicarboxylate as an aromatic biobased monomer toward lipase-catalyzed synthesis of semiaromatic copolyesters, ACS Appl. Polym. Mater. 4 (2022) 1387–1400, https://doi.org/10.1021/acsapm.1c01777.
[23] V. Tsanaktsis, Z. Terzopoulou, M. Nerantzaki, G.Z. Papageorgiou, D.N. Bikiaris, New poly(pentylene furanoate) and poly(heptylene furanoate) sustainable polyesters from diols with odd methylene groups, Mater. Lett. 178 (2016) 64–67, https://doi.org/10.1016/j.matlet.2016.04.183.
[24] G. Guidotti, M. Soccio, M.C. García-Gutiérrez, E. Gutiérrez-Fernández, T. A. Ezquerra, V. Siracusa, A. Munari, N. Lotti, Evidence of a 2D-ordered structure in biobased poly(pentamethylene furanoate) responsible for its outstanding barrier and mechanical properties, ACS Sustain. Chem. Eng. 7 (2019) 17863–17871, https://doi.org/10.1021/acssuschemeng.9b04407.
[25] G. Guidotti, M. Soccio, M.C. García-Gutiérrez, T. Ezquerra, V. Siracusa, E. Gutiérrez-Fernández, A. Munari, N. Lotti, Fully biobased superpolymers of 2,5-furandicarboxylic acid with different functional properties: from rigid to flexible, high performant packaging materials, ACS Sustain. Chem. Eng. 8 (2020) 9558–9568, https://doi.org/10.1021/acssuschemeng.0c02840.
[26] M. Jiang, Q. Liu, Q. Zhang, C. Ye, G. Zhou, A series of furan-aromatic polyesters synthesized via direct esterification method based on renewable resources, J. Polym. Sci. A Polym. Chem. 50 (2012) 1026–1036, https://doi.org/10.1002/pola.25859.
[27] V. Tsanaktsis, G.Z. Papageorgiou, D.N. Bikiaris, A facile method to synthesize high-molecular-weight biobased polyesters from 2,5-furandicarboxylic acid and long-chain diols, J. Polym. Sci. A Polym. Chem. 53 (2015) 2617–2632, https://doi.org/10.1002/pola.27730.
[28] M. Lomelí-Rodríguez, J.R. Corpas-Martínez, S. Willis, R. Mulholland, J.A. Lopez-Sanchez, Synthesis and characterization of renewable polyester coil coatings from biomass-derived isosorbide, FDCA, 1,5-pentanediol, succinic acid, and 1,3-propanediol, Polymers (basel) 10 (2018), https://doi.org/10.3390/polym10060600.
[29] E. Bianchi, G. Guidotti, M. Soccio, V. Siracusa, M. Gazzano, E. Salatelli, N. Lotti, Biobased and compostable multiblock copolymer of poly(l-lactic acid) containing 2,5-furandicarboxylic acid for sustainable food packaging: the role of parent homopolymers in the composting kinetics and mechanism, Biomacromolecules 24 (2023) 2356–2368, https://doi.org/10.1021/acs.biomac.3c00216.
[30] G. Guidotti, M. Soccio, V. Siracusa, M. Gazzano, E. Salatelli, A. Munari, N. Lotti, Novel random PBS-based copolymers containing aliphatic side chains for sustainable flexible food packaging, Polymers (Basel) 9 (2017), https://doi.org/10.3390/polym9120724.
[31] J. Devaux, P. Godard, J.P. Mercier, Bisphenol-A Polycarbonate-Poly(butylene Terephthalate) Transesterification. I. Theoretical Study of the Structure and of the Degree of Randomness in Four-Component Copolycondensates, n.d.
[32] Y.-K. Han, S.-R. Kim, J. Kim, Preparation and Characterization of High Molecular Weight Poly(butylene succinate) †, 2002.
[33] T.X. Jin, M. Zhou, S.D. Hu, F. Chen, Q. Fu, Y. Fu, Effect of molecular weight on the properties of poly(butylene succinate), Chin. J. Polym. Sci. (Engl. Ed.) 32 (2014) 953–960, https://doi.org/10.1007/s10118-014-1463-4.
[34] M.C. Righetti, M.L. Di Lorenzo, D. Cavallo, A.J. Müller, M. Gazzano, Structural evolution of poly(butylene succinate) crystals on heating with the formation of a dual lamellar population, as monitored by temperature-dependent WAXS/SAXS analysis, Polymer (Guildf) 268 (2023), https://doi.org/10.1016/j.polymer.2023.125711.
[35] G. Guidotti, M. Soccio, V. Siracusa, M. Gazzano, A. Munari, N. Lotti, Novel random copolymers of poly(butylene 1,4-cyclohexane dicarboxylate) with outstanding barrier properties for green and sustainable packaging: Content and length of aliphatic side chains as efficient tools to tailor the material's final performance, Polymers (Basel) 10 (2018), https://doi.org/10.3390/polym10080866.
[36] Y. Yang, Z. Qiu, Crystallization kinetics and morphology of biodegradable poly (butylene succinate-co-ethylene succinate) copolyesters: effects of comonomer composition and crystallization temperature, CrstEngComm 13 (2011) 2408–2417, https://doi.org/10.1039/c0ce00598c.
[37] D. Rigotti, M. Soccio, A. Dorigato, M. Gazzano, V. Siracusa, G. Fredi, N. Lotti, Novel biobased polylactic acid/poly(pentamethylene 2,5-furanoate) blends for sustainable food packaging, ACS Sustain. Chem. Eng. 9 (2021) 13742–13750, https://doi.org/10.1021/acssuschemeng.1c04092.
[38] G. Guidotti, M. Soccio, M. Gazzano, N. Bloise, G. Bruni, A. Aluigi, L. Visai, A. Munari, N. Lotti, Biocompatible PBS-based copolymer for soft tissue engineering: Introduction of disulfide bonds as winning tool to tune the final properties, Polym. Degrad. Stab. 182 (2020), https://doi.org/10.1016/j.polymdegradstab.2020.109403.
[39] A.K. Bhargava, C.P. Sharma, Mechanical Behaviour and Testing of Materials, second ed., 2011.
[40] X. Zhou, J. Wu, D. Yu, Study on tensile stress fluctuation of poly(butylene succinate) (PBS) and its bicrystalline block copolyesters (PBSEG), Polym. Eng. Sci. 64 (2024) 101–107, https://doi.org/10.1002/pen.26531.
[41] C. Wan, E.L. Heeley, Y. Zhou, S. Wang, C.T. Cafolla, E.M. Crabb, D.J. Hughes, Stress-oscillation behaviour of semi-crystalline polymers: the case of poly(butylene succinate), Soft Matter 14 (2018) 9175–9184, https://doi.org/10.1039/C8SM01889H.
[42] C.C. Sarath, R.A. Shanks, S. Thomas, Polymer Blends, in: Nanostructured Polymer Blends, Elsevier Inc., 2013: pp. 1–14. https://doi.org/10.1016/B978-1-4557-3159-6.00001-8.
[43] G. Markovic, P.M. Visakh, Polymer blends: State of art, in: Recent Developments in Polymer Macro, Micro and Nano Blends: Preparation and Characterisation, Elsevier Inc., 2017: pp. 1–15. https://doi.org/10.1016/B978-0-08-100408-1.00001-7.
[44] G. Mensitieri, E. Di Maio, G.G. Buonocore, I. Nedi, M. Oliviero, L. Sansone, S. Iannace, Processing and shelf life issues of selected food packaging materials and structures from renewable resources, Trends Food Sci. Technol. 22 (2011) 72–80, https://doi.org/10.1016/j.tifs.2010.10.001.